IET Renewable Power Generation

Special Issue Call for Papers

Be Seen. Be Cited.
Submit your work to a new IET special issue

Connect with researchers and experts in your field and share knowledge.

Be part of the latest research trends, faster.

Read more

The Institution of Engineering and Technology

Received: 27 May 2022 | Revised: 9 February 2023 | Accepted: 10 March 2023

DOI: 10.1049/rpg2.12721

IET Renewable Power Generation

The Institution of Engineering and Technology WILEY

ORIGINAL RESEARCH

A comparison study of power performance and extreme load effects of large 10-MW offshore wind turbines

Shuaishuai Wang[1] | **Yihan Xing**[2] | **Anuraj Karuvathil**[2] | **Oleg Gaidai**[3]

[1]Norwegian University of Science and Technology, Trondheim, Norway

[2]Department of Mechanical and Structural Engineering and Materials Science, University of Stavanger, Stavanger, Norway

[3]Shanghai Engineering Research Centre of Marine Renewable Energy, College of Engineering Science and Technology, Shanghai Ocean University, Shanghai, China

Correspondence
Shuaishuai Wang, Norwegian University of Science and Technology, Trondheim, Norway.
Email: shuaishuai.wang@ntnu.no

Abstract

The utilisation of offshore wind turbines has rapidly increased in the last decade, which has resulted in a steady increase in wind turbine sizes. The global average offshore wind turbine size has increased from 1.5 MW to 6 MW in the last two decades. The research community has started to investigate huge 10 to 15 MW offshore wind turbines in recent years, resulting in the study of very innovative floating wind turbines using various substructure technologies. With this backdrop, this paper will investigate and thoroughly compare the power performance of extreme load effects of a large offshore 10 MW turbine installed on the monopile, spar, and semisubmersible substructures. This is performed by using the average conditional exceedance rate (ACER) and Gumbel methods to predict the extreme responses under the operating conditions of 8, 12, and 16 m/s mean wind speed, representing the below-rated, rated, and above-rated regions, respectively. The results show that the power performance and extreme loads experienced depends significantly on the operating regions. The mean power generation between the three different types of offshore wind turbines (OWTs) are closely in the whole operating range, which standard deviations differ significantly. Large standard deviations of power generation appear in the spar turbine under the below-rated condition. Further, it was observed that the spar wind turbine generally experiences larger extreme loads due to larger platform pitch motion. In addition, the ACER method shows a better prediction for the 1, 2 and 5-year extreme responses than the Gumbel method, which is due to the relatively poor data fitting of the Gumbel method at the upper tail. The study is believed to consolidate and close the knowledge gap in understanding wind turbine responses across the most common offshore substructure technologies and provide a basis for design and deployment of OWTs.

1 | INTRODUCTION

Low-carbon technologies have been becoming essential because they can effectively facilitate the transformation from fossil fuels to renewable energy and thus promote the realisation of the global sustainable energy goal. Wind power is one of the significant renewable energy sources in accelerating the global energy transition. Even though the onshore wind market dominates, offshore wind power demonstrates excellent potential for rapid development due to the vast untapped resources.

According to the substructure type, offshore wind turbines (OWTs) can be categorised by fixed types, such as Triple, Tripod, Gravity base, Jacket, Monopile; and floating types, such as spar, semisubmersible, barge, and tension-leg platform (TLP). In the offshore wind report by Wind Europe [1], by the early 2021, Monopile OWT in Europe reached a cumulative 4681 units and remained the most used type with a market share of approximately 81.2%. In contrast, all floating wind turbines (FOWTs) account for only about 0.2% of total units. This is because FOWTs are usually installed at distant shore locations where the wind resources are more stable and abundant than the near coast; the installations of the bottom-fixed offshore turbine in regions with water depth exceeding 50–60 m are not economically attractive [2]. However, floating offshore wind has been attracted significant attention in recent years and shows a massive prospect for rapid development.

To promote the successful evolvement of offshore wind from shallow water to deep water regions, a significant reduction of the levelized cost of energy (LCOE) is necessary. FOWTs are generally based on classical substructure design, such as the spar, semisubmersible, and TLP, developed by learning from the oil and gas industry [3]. However, different design criteria are needed to design OWT substructures compared to the offshore oil and gas platforms. This is because offshore oil and gas platforms mainly withstand wave loads, while OWTs also have to withstand substantial wind loads. OWTs are usually designed following the international standard IEC 61400–3 [4], covering additional wave, current, and tidal conditions in the general sea states. However, the IEC 61400–3 standard cannot be used as the basis for FOWT design yet.

Compared to the bottom-fixed OWTs, FOWTs are still in the early stage of technology, mainly due to the superficial understanding of complex dynamics. FOWTs present strong nonlinearity in the dynamic behaviour because of the interactions of the aerodynamic and hydrodynamic loads, the structural flexibility, the advanced controller system, and the stochastic turbulent wind and irregular wave conditions. In addition, various conditions, including start-up, normal operating, faulted and emergent shutdown, and parked conditions, increase the complexity of the dynamic behaviour of FOWTs.

The power and dynamic load effect performance of OWTs differ in different substructure supports, which have been presented in several studies, i.e., [5–9]. Although these studies addressed specific dynamic analysis for different OWTs, the focuses are different and limited, and much more efforts need to be devoted to getting more profound insight into the dynamic behaviour of FOWTs, which will be the basis for technology improvement and LCOE reduction. Extreme response analysis is an essential aspect of OWTs because the extreme responses are the basis for the ultimate limit state (ULS) check, a fundamental criterion for OWT structural design. Aggarwal et al. [10] studied 3-h short term extreme motions for a 5-MW spar-type FOWT. Chen et al. [11] presented a modified environmental contour method (MECM) for long-term extreme response analysis of OWTs. Tower base and monopile extreme loads of a 5-MW bottom-fixed OWT estimated by full long-term analysis, ECM, and MECM methods were compared, and the results showed that the proposed MECM could achieve a more accurate prediction of the extreme structural loads than the traditional ECM. An averaged conditional exceedance rate (ACER) method was introduced and described in the reference [12] based on the method developed by Naess and Gaidai [13]. The ACER method is less restrictive and more flexible than the approaches based on asymptotic theory, and it is capable of capturing subasymptotic behaviour of data and is applicable to nonstationary time series. The ACER extrapolation method has been successfully applied and validated for the extreme value prediction, i.e., on the mean up-crossing rate function tail of many engineering problems including wind turbine applications, e.g., [14–17].

However, there is a lack of comparison of extreme responses between different support type OWTs, which can be an essential basis in contributing to the improvement of the design guidelines for OWTs. To close this knowledge gap, this study proposes a comparative study of the power generation and extreme response analysis for three 10-MW OWTs supported on the bottom-fixed, spar, and semisubmersible substructures, respectively.

2 | FLOATING WIND TURBINE CONCEPTS

Three 10-MW offshore wind turbine concepts: a monopile bottom-fixed, a spar and a semisubmersible type, are used in this study. The Technical University of Denmark (DTU) 10-MW reference wind turbine (RWT) [18] is employed in the three offshore concepts, which were developed by upscaling from the National Renewable Energy Laboratory (NREL) 5-MW wind turbine but emphasised the optimised design of the rotor blades. The 10-MW RWT is a three-bladed upwind clockwise rotating wind turbine with varying speed pitch control arrangement… The wind turbine is designed with a cut in speed of 4 m/s, a rated speed of 11.4 m/s and a cut-out speed of 25 m/s. In addition, the minimum and maximum rotor speeds are 6.0 rpm and 9.6 rpm, respectively. More detailed information about the DTU 10-MW RWT can be found in the technical report [18].

The sketches of the monopile-, spar- and semi-submersible-type offshore wind turbines are illustrated in Figure 1. Each offshore wind turbine concept is described in greater detail in Sections 2.1–2.3, respectively.

2.1 | Bottom-fixed monopile concept

The 10-MW bottom-fixed monopile wind turbine concept used in the present work was designed by Velarde and Bachynski [19]. The monopile foundation was designed for a water depth of 30 m. Parameters of the pile diameter, thickness, penetration depth of the monopile foundation, and the tower material, diameter, and thickness are determined to obtain the desired natural frequency. The desired natural frequency of the monopile turbine structure is in a soft-stiff region and falls outside the blade 1P and 3P excitation regions to avoid structural resonance. A natural frequency of 0.251 Hz was realised based on the design considerations. Detailed specifications of the monopile-support wind turbine are illustrated in Figure 1a and are presented in the paper [19].

2.2 | Spar-type floating concept

Hegseth and Bachynski [20] designed the spar platform for supporting the 10-MW RWT. The spar support structure was developed from the OC3-Hywind spar concept [21], but the draft of the hull for the 10-MW RWT model was reduced to 90 m to make it applicable in intermediate water depths. To improve the hydrodynamic stability and buoyancy, the diameter

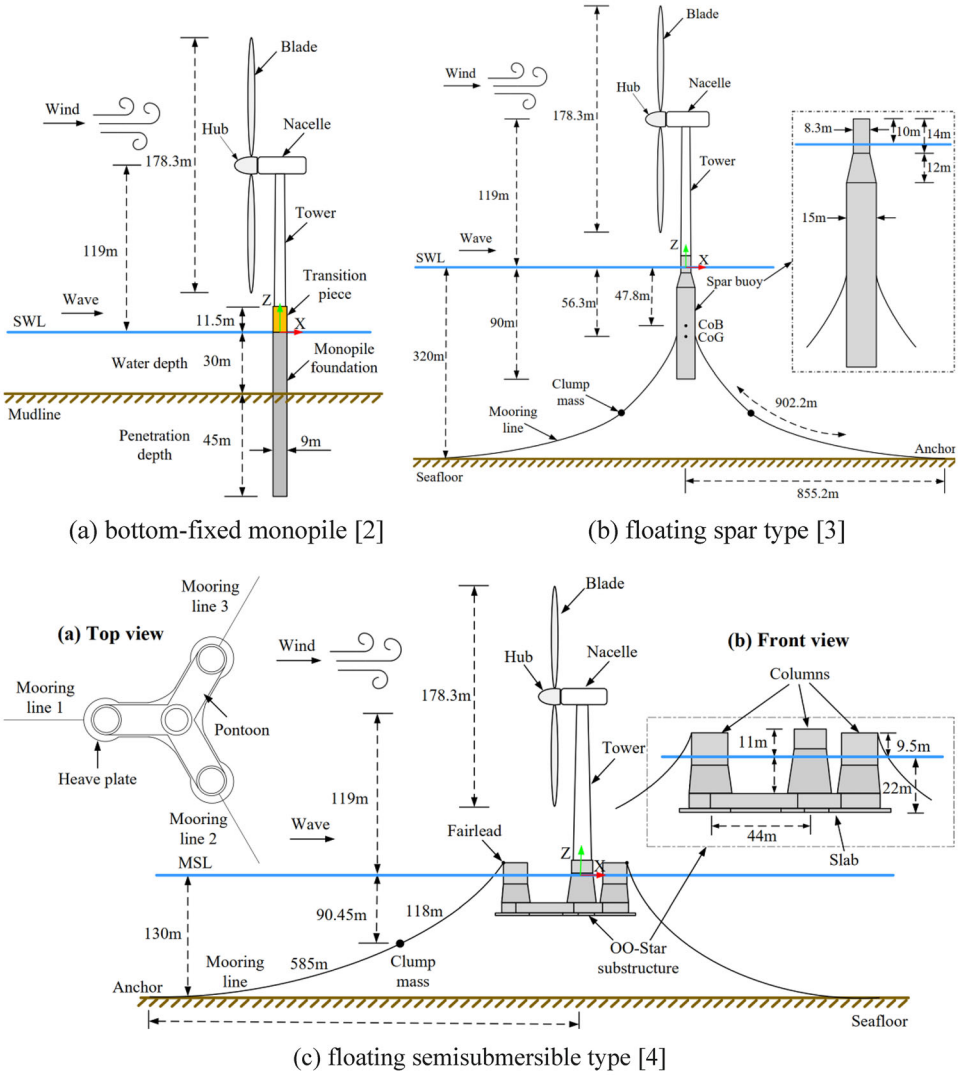

FIGURE 1 Sketches of the 10-MW bottom-fixed monopile, floating spar-, and semisubmersible types offshore wind turbine concepts. (a) Bottom-fixed monopile [2]; (b) floating spar type [3]; (c) floating semisubmersible type [4].

of the hull and the ballast mass was increased. A heavy ballast was also placed at the bottom of the hull to improve stability.

The spar platform consists of two cylinders with different diameters and is connected by a taper section, as illustrated in Figure 1b. The tower length and bottom diameter are modified from the DTU 10-MW RWT to join the spar platform. As a result, the dimensions of the tower sections are adjusted accordingly to maintain the same hub height as the land-based RWT; meanwhile, to make the natural frequencies in tower bending moment modes above the rotor 3P excitation range.

The spar-type floating wind turbine with the catenary mooring system improves the yaw stiffness by using a rotational spring. The fairleads are placed at the centre of gravity (COG) to reduce the coupling of surge and pitch motions. The 10-MW spar-type floating wind turbine was introduced in greater detail in Figure 1b and the reference [20]. The natural frequency properties of the spar model can be found in the papers [8, 20], which will be useful to facilitate a better understanding of the dynamic analysis results.

2.3 | Semisubmersible type floating concept

The semisubmersible platform for supporting the 10-MW Reference Wind Turbine was designed and developed by Dr.techn. Olav Olsen as described in the LIFES 50+ project [22]. In the LIFES 50+ project, two semisubmersible concrete concepts were designed, and the OO-Star concrete concept is used iFn the present work. The OO-Star platform consists of three outer columns and a central column where the turbine is installed on the central column. The four columns are mounted on three pontoons, and each pontoon connects an outer column and the main column. A heave plate is attached at the bottom of the pontoons to increase the natural heave period.

Because the central column of the platform has an 11 m height above the mean sea level, the tower length is shortened accordingly to maintain the same hub height of the land-based RWT. Moreover, the outer diameter of the tower bottom is modified to match the interface of the platform's central column. Then, the wall thickness and outer diameter of each tower

segment were adjusted to avoid the resonance of the coupled tower-platform structure.

Three catenary mooring lines are used for station keeping, and the horizontal angle between two adjacent lines is 120 degrees. A clumped mass is attached to each mooring line to increase the mooring tension. More details of the OO-Star semisubmersible FOWT system are demonstrated in Figure 1c and in the LIFES50+ project reports [22, 23].

The main properties of the monopile foundation, floating support structures and mooring systems of the three 10-MW OWTs are organized and listed in the reference [24].

3 | METHODOLOGY

3.1 | Aero-hydro-servo-elastic dynamic analysis of the 10-MW OWT models

The aero-hydro-servo-elastic fully coupled numerical analysis of the 10-MW monopile, spar, and semisubmersible OWT models are carried out by using the simulation tool SIMA [25]. SIMA is sophisticated software for marine operations and mooring analysis, and it has been successfully used for bottom-fixed and floating OWT dynamic analysis. The simulation tool integrates two computer codes: SIMO and RIFLEX. SIMO calculates the hydrodynamic loads and dynamic motions of floating structures. RIFLEX is a nonlinear finite element solver for calculating the structural responses of flexible elements, and it also provides an external controller for blade pitch and shaft torque controls. The simulation software can reasonably account for the aerodynamics, hydrodynamics, structural dynamics, and control system dynamics for OWT analysis.

The identical rotor, hub, and nacelle are used in the monopile, spar and semisubmersible OWT models. The hub, nacelle, spar and semisubmersible floating platforms are considered rigid bodies. The blades, tower, shaft and monopile are modelled by nonlinear beams. Nonlinear p-y curves model the laterally of the monopile below the mud line. Mooring lines in the spar and semisubmersible FOWTs are modelled by nonlinear bar elements, where only the axial stiffness is considered.

Blade element momentum theory is used to calculate the forces on the wind turbine. The momentum theory refines the induced velocities calculation is used to analyse the aerodynamics loads on the rotor of the monopile, spar and semisubmersible. Advanced corrections include Prandtl and Glauert for hub and tip loss, dynamic wake correction, tower shadow, dynamic stall, and skewed inflow corrections.

Hydrodynamic loads on the monopile and mooring lines are calculated based on Morison's equation, where both the drag and inertial terms are included. The hydrodynamic loads on the spar and semisubmersible hulls are computed using the potential flow theory and Morison's equation. First-order wave loads on the structural hulls are first obtained in the panel model's frequency domain; then, they are applied in the time domain using the convolution techniques. The drag term of Morison's equation is used to account for the viscous forces omitted in the potential flow theory in the two FOWTs.

The control system for the three OWT models consists of the blade pitch control and the generator torque control, and they are written in JAVA and applied through the interface in RIFLEX. The proportional and integral coefficients, *KP* and *KI*, of the controller in the monopile OWT are those of the original values used in the onshore RWT. However, the controller coefficients used in the spar and semisubmersible FOWTs are modified to avoid the negative damping effect and thus prevent unstable pitch motions.

3.2 | Extreme value prediction

In any stochastic process $X(t)$ taken across a period (T), the extreme value is the largest maxima extracted from a group of individual maxima [11].

$$X_e = max\{X_{m1}, X_{m2}, X_{m3}, \dots, X_{mn}\}\ ,\ i = 1, \dots, n, \quad (1)$$

where X_e describes the largest maximum value and X_{mi} describes the individual maxima. Therefore, from this assumption, it is observed that the individual maxima are independently and identically distributed across the common distribution function $F_{Xm}(x)$. Thus, from the equation below, the distribution of X_e is labelled as [11]:

$$F\ (x) = Prob\ \{X_e \le x\} = \left[F_{Xm}\ (x)\right]^n\ ,\ i = 1, \dots, n. \quad (2)$$

Various statistical methods have been used to approximate an extreme value distribution. Examples of the extreme value methods used in the study of wind turbines include an estimation of extreme structural responses in floating vertical axis wind turbines by Cheng et al. [26] and extreme responses due to wave irregularity on an offshore floating wind turbine by Xu et al. [27]. The two popular techniques used in this paper are the ACER method (Section 3.3) and the Gumbel method (Section 3.4).

3.3 | ACER (average conditional exceedance rate)

This paper uses the ACER method to estimate extreme structural responses. The method was proposed by Naess and Gaidai [13], and it is derived for a discretely sampled response process. The cascade of conditional approximation is the basis for calculating the exceedance probability for extreme value estimation. The primary purpose of the ACER method is to accurately determine the distribution function of the extreme value, which is denoted as $M_N = max\{X_j;\ j = 1, \cdots, N\}$. Let $P_\eta = Prob(M_N \le \eta)$ denotes the probability of the occurrence of the extreme value η and it follows [11, 12]:

$$P_\eta = Prob\ (M_N \le \eta) = Prob\,(X_1 \le \eta,\ \cdots,\ X_N \le \eta)\,. \quad (3)$$

To solve this equation efficiently, a cascade of conditional approximation $P_k(\eta)$ is used, where $P_k(\eta)$ tends to be close to P_η

as k increases. For N'' 1 and$k = 1, 2, \cdots, P_k(\eta)$ is represented as [11, 12]:

$$P_k(\eta) \approx exp\left(-\sum_{j=k}^{N} \alpha_{kj}(\eta)\right), \quad (4)$$

where $\alpha_{kj}(\eta) = Prob(X_1 > \eta | X_{j-1}{}''\eta, \ldots, X_{j-k+1} \le \eta)$ And it represents the exceedance probability conditional on $k-1$ previous non-exceedances.

Equation (4) will be calculated based on the ACER, which is defined as [11, 12]:

$$\varepsilon_k(\eta) = \frac{1}{N-k+1} \sum_{j=k}^{N} \alpha_{kj}(\eta), k = 1, 2, \ldots . \quad (5)$$

For $k \ge 2$, $\tilde{\varepsilon}_k(\eta)$ is used instead of $\varepsilon_k(\eta)$ because it is easier to use for nonstationary or long-term statistics, and it is defined as [11, 12]:

$$\hat{\varepsilon}_k(\eta) = \lim_{N\to\infty} \frac{\sum_{j=k}^{N} a_{kj}(\eta)}{N-k+1}, \quad (6)$$

where $a_{kj}(\eta)$ is the realised values for the observed time series, and $\lim_{N\to\infty} \frac{\hat{\varepsilon}_k(\eta)}{\varepsilon_k(\eta)} = 1$.

For both stationary and nonstationary time series, the sample estimate of the ACER can be denoted as [11, 12]:

$$\hat{\varepsilon}_k(\eta) = \frac{1}{R} \sum_{r=1}^{R} \hat{\varepsilon}_k^{(r)}(\eta), \quad (7)$$

where R is the number of samples, and [11, 12]

$$\hat{\varepsilon}_k^{(r)}(\eta) = \frac{\sum_{j=k}^{N} a_{kj}{}^{(r)}(\eta)}{N-k+1}, \quad (8)$$

where r denotes the realisation number.

When the realisations are sufficiently numerous and assumed to be independent, then the 95 % confidence interval (CI) for the ACER can be estimated as [11, 12]:

$$CI(\eta) = \hat{\varepsilon}_k(\eta) \pm 1.96\, \hat{s}_k(\eta) / \sqrt{R}, \quad (9)$$

where $\hat{s}_k(\eta)$ refers to the standard deviation of samples and can be estimated by [11, 12]:

$$\hat{s}_k(\eta)^2 = \frac{1}{R-1} \sum_{r=1}^{R} \left(\hat{\varepsilon}_k^{(r)}(\eta) - \hat{\varepsilon}_k(\eta)\right)^2. \quad (10)$$

The above equations for estimation of average exceedance rate are based on direct numerical simulations. In contrast, an extrapolation technique can reduce the computational time.

Assuming the mean exceedance rate in the tail behaves similarly to $exp\{-a(\eta - b)^c\}(\eta \ge \eta_0 \ge b)$, where a, b and c are suitable constants. The ACER will therefore be assumed by [11, 12]:

$$\varepsilon_k(\eta) \approx q_k(\eta)\, exp\left\{-a_k(\eta - b_k)^{c_k}\right\}, \eta \ge \eta_0, \quad (11)$$

where the function $q_k(\eta)$ varies slowly compared to the exponential function $exp\{-a_k(\eta - b_k)^{c_k}\}$ in the tail region, thus it can be replaced by a constant for a suitable choice of the tail marker η_0.

Finally, the Levenberg-Marquardt least-squares optimisation method can be used to determine the constants a, b, c and q. Based on this, the probability of the occurrence of the extreme value can be obtained by the ACER method. In the studies of Naess et al. [28] and Chai et al. [29] it is shown that the extrapolation technique can achieve a satisfactory estimation of the extreme values but saves significant simulation time. Detailed descriptions of the ACER method can be found in the reference [12].

3.4 | Gumbel fitting method

Extreme value distribution Equation (2) has been proven to converge to the Gumbel, Fréchet or Weibull distribution if the sample size (n) is large enough. Therefore, these distributions are also recognised as the Type I, II and III extreme value distributions, respectively and are a family of cumulative distribution probability that combines the generalised extreme value (GEV) distribution. More details about the following Equations can be found in the reference [11].

$$F_{X_e}(x) = exp\left(-\left(1 + \gamma\left(\frac{x-\mu}{\beta}\right)\right)^{-\frac{1}{\gamma}}\right), \quad (12)$$

where β describes the scale parameter, γ describes the shape parameter, and μ represents the location parameter. The limiting of $\gamma \to 0$ allows the approximation to fit the Gumbel distribution, commonly used as a recommendation when modelling marine structures [30].

$$F_{X_e}(x) = exp\left(-exp\left(-\frac{x-\mu}{\beta}\right)\right). \quad (13)$$

Equation (13) can be rewritten by using a logarithm on the equation, allowing it to become a linear function.

$$-ln\left(ln\left(F_{X_e}(x)\right)\right) = \frac{x}{\beta} - \frac{\mu}{\beta}. \quad (14)$$

The parameters β and μ can be approximated from the original data using the least-square fitting method from the cumulative distribution probability, that is, a straight line on a probability paper [31].

3.5 | Environmental conditions and load cases

The environmental conditions at site 14 in the Northern part of the North Sea are used in the presented work, where the 10-MW FOWT is assumed to be installed. The environmental

data are selected from a long-term joint distribution of mean wind speed at 10 m height above the sea level (U_{10}), significant wave height (H_s), and spectral peak period (T_p). The wind and wave distribution was developed by a hindcast model using the measured raw data from 2001-to 2010 of the location as a database, as proposed in the study of Li et al. [32].

The long-term joint wind and wave distribution can be written as:

$$f_{U_{10},H_s,T_p}(u,h,t) = f_{U_{10}}(u) \cdot f_{H_s|U_{10}}(h|u) \cdot f_{T_p|U_{10},H_s}(t|u,h), \tag{15}$$

where $f_{U_{10}}(u)$ represents the marginal distribution of the 1-h mean wind speed U_{10}, $f_{H_s|U_{10}}(h|u)$ denotes the conditional distribution of H_s for given U_{10}, *and* $f_{T_p|U_{10},H_s}(t|u,h)$ represents the conditional distribution of T_p for given U_{10} and H_s.

A two-parameter Weibull distribution represents the marginal distribution of the U10, and the probability density function (PDF) is given by [32]:

$$f_{U_{10}}(u) = \frac{\alpha_U}{\beta_U}\left(\frac{u}{\beta_U}\right)^{\alpha_U-1} exp\left[-\left(\frac{u}{\beta_U}\right)^{\alpha_U}\right], \tag{16}$$

where α_U and β_U represent the shape and scale parameters, and they are 2.029 and 9.409, respectively, for the specific sea location.

A two-parameter Weibull distribution describes the conditional PDF of Hs for given U10 [32]:

$$f_{H_s|U_{10}}(h|u) = \frac{\alpha_{HC}}{\beta_{HC}}\left(\frac{u}{\beta_{HC}}\right)^{\alpha_{HC}-1} exp\left[-\left(\frac{u}{\beta_{HC}}\right)^{\alpha_{HC}}\right], \tag{17}$$

where α_{HC} and β_{HC} are the shape and scale parameters, respectively, and they are expressed by power functions of mean wind speed [32]:

$$\begin{aligned} \alpha_{HC} &= a_1 + a_2 u^{a_3} \\ \beta_{HC} &= b_1 + b_2 u^{b_3}, \end{aligned} \tag{18}$$

where $a_1 = 2.136$, $a_2 = 0.013$, $a_3 = 1.709$, $b_1 = 1.816$, $b_2 = 0.024$, $b_3 = 1.787$ are the parameters for estimating the α_{HC} and β_{HC}.

The conditional PDF of T_p for given U_{10} and H_s is fitted by a lognormal distribution [32]:

$$f_{T_p|U_{10},H_s}(t|u,h) = \frac{1}{\sqrt{2\pi}\sigma_{ln(T_p)}t} exp\left[-\frac{1}{2}\left(\frac{ln(t)-\mu_{ln(T_p)}}{\sigma_{ln(T_p)}}\right)^2\right], \tag{19}$$

where $\mu_{ln(T_p)}$ *and* $\sigma_{ln(T_p)}$ are the parameters in the conditional lognormal distribution and they are estimated by a detailed analysis in the study of Li et al. [32].

Three representative environmental conditions using U_{10}, H_s and T_p are considered in this paper. Correspondingly, different load cases with irregular wind and waves are analysed to study the power performance and extreme responses of the three OWTs. Mean wind speeds at the hub height are estimated based on the power-law formulation, as follows [32]:

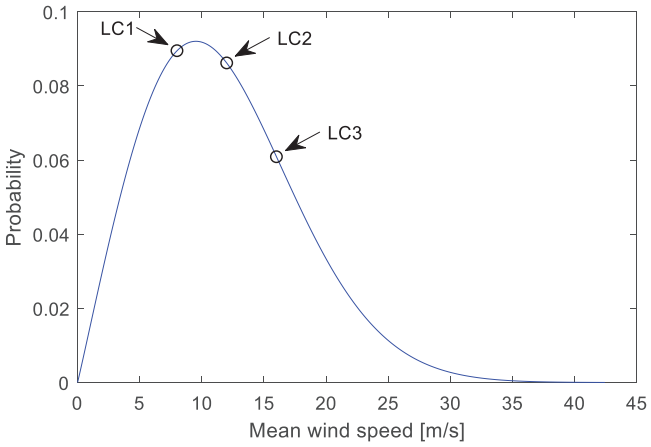

FIGURE 2 PDF of the average wind speed at wind turbine hub height.

$$U_{10} = U_{hub}\left(\frac{10}{Z_{hub}}\right)^{\alpha}, \tag{20}$$

where U_{hub} and U_{10} are the mean wind speeds at the hub height and 10 m height above the sea level, respectively. $Z_{hub} = 119$ m is the hub height of the 10-MW OWTs. According to international standard IEC 61400–3, the exponent in the power law is set at 0.14.

The load cases for numerical simulations are listed in Table 1. The average wind speeds of 8, 12, and 16 m/s at the hub height are chosen to account for the dynamics of the wind turbines under the cut-in, rated, and above rated operating zones illustrated in Figure 2. For each given mean wind speed, the maximum probable H_s and T_p are selected according to the joint distributions of U_{10}, H_s and T_p.

The turbulent wind fields are generated using the Turbsim program according to Kaimal's turbulence model defined in IEC 61400–3 [4]. Meanwhile, the JONSWAP (Joint North Sea Wave Project) spectrum modulates the time-varying irregular waves with the respective H_s and T_p values. Wind and waves are considered to be directionally aligned in this work.

Each simulation lasted for a period of 4000 s. To remove the transient effects in the wind turbine during startup, the starting 400 s readings were eliminated. Consequently, one-hour data for each simulation is used for studying the results. 20 random wind and wave samples are considered for each environmental condition to account for the stochastic uncertainties. The power performance and extreme values are assessed based on the mean of the twenty 1-h simulations.

4 | RESPONSE VARIABLES

The loads at the eight measurement points are considered. These are the tower My and Mz bending moment, blade 1 My and Mz bending moment, blade 2 My and Mz bending

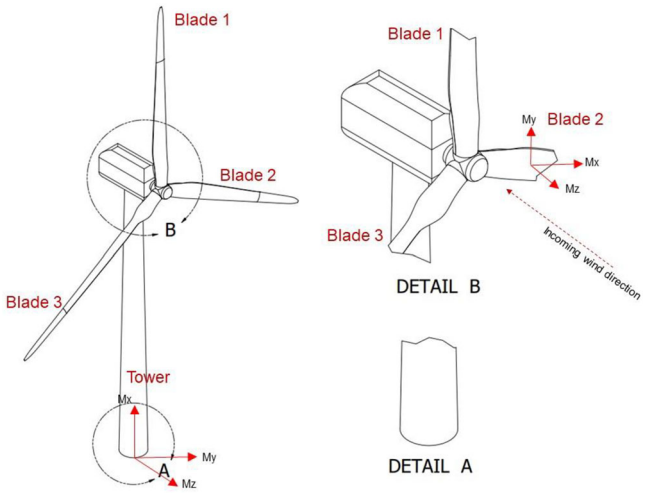

FIGURE 3 Bending moment measured locations.

moment and blade 3 My and Mz bending moment, as illustrated in Figure 3 as follows.

5 | RESULTS AND DISCUSSIONS

The empirical data is based on accurate numerical simulations using a SIMA model as presented in Section 3.1. The Gumbel and ACER methods presented in Sections 3.3 and 3.4 are used.

5.1 | Time-domain responses, PSD, and maximum values

In this section, dynamic characteristics of the tower-bottom and blade root bending moments of the three OWTs are compared and investigated. The one-hour time-domain responses and the power spectral densities (PSDs) for a full realisation and the maximum values of each realisation are presented in Figures 4, 5, and 6, respectively. The LC2 is considered to illustrate the dynamic characteristics.

It is observed from the time domain responses represented in Figure 4 that the tower bottom responses of the monopile wind turbine are smaller than those of the spar and semi-submersible wind turbines. In contrast, the blade root bending moments between the three OWTs are close. The main reason is that the spar and semi-submersible platforms have significant pitch motions, while the monopile wind turbine is a fixed type offshore wind turbine with negligible pitch motion responses. More details will be revealed by the PSD analysis in the following.

Referring to Figure 5, the PSDs for the tower bottom and blade root bending moments between the monopile, spar, and semisubmersible wind turbines are compared under the LC2. Significant response exists in the spar wind turbine at the tower bottom bending moment My compared to the monopile and semi-submersible wind turbines. The large responses are caused by the significant pitch motion of the spar floating wind turbine, as shown in the top-left PSD result, which is mainly induced by the low frequency wind loads. Meanwhile, the roll motion induced responses are dominating in the tower bottom bending moment Mz of the spar and semi-submersible FOWTs, while the responses of the monopile turbine are negligible. The dynamic characteristics of the blade root bending moment My are very close for blade1, blade2, and blade3, but they differ between the monopile, spar, and semi-submersible wind turbines. Significant response of the monopile turbine is located at the frequency of blade rotation, which is dramatically larger than that of the spar and semi-submersible turbines. However, the responses at the low-frequencies are converse for the monopile and the other two floating wind turbines. This is because that the low frequency motions of the spar and semi-submersible floaters induced by the wind loads significantly contribute to the aerodynamic loads, thereby the blade root bending moments.

Several detailed observations can be made on the maximum values presented in Figure 6. The maximum values of the structural responses are closely associated with the controller properties, dynamic motion properties and tower vibrations etc. In general, the floating wind turbines have significantly larger maximum values for most of the responses considered expect for the tower My bending moment; the monopile wind turbine has the smallest maximum values. For example, the blade My bending moments for the floating wind turbines are about 20% larger than the fixed wind turbine. Further, the variation of the maximum values of the floating wind turbines is also significantly larger than the monopile wind turbine. For example, for the blade My bending moments, the variation for the floating wind turbines is about 10 %, while for the fixed wind turbine, they are about 5%.

5.2 | Comparison of power performance

The power production values are presented in Figure 7 for the three environmental conditions. The mean values are presented on the left, while the standard deviations are presented on the right. The probability of the occurrence of the environmental conditions 8, 12, and 16 m/s are 0.0895, 0.0864, and 0.0611, respectively, which are selected from the Figure 2 based on the Equation (16).

It is observed that the mean power production values are about 5% smaller for the spar concept compared to the fixed and semisubmersible turbines. This can be explained as follows. The spar turbine has a relatively small hydrostatic restoring pitch moment. The spar platform will have a mean pitch angle of some five degrees during operation. This mean pitch angle causes the rotor plane normal to be slightly out of the plane with the incoming wind, leading to less optimal power production. In contrast, the semisubmersible platform has a large hydrostatic restoring pitch moment due to the moment arms provided by the distance between the platform centre and the pontoon. This large hydrostatic restoring pitch moment leads to a small mean platform pitch angle. Therefore, the incoming wind will be aligned to the normal rotor plane, giving more optimal power production.

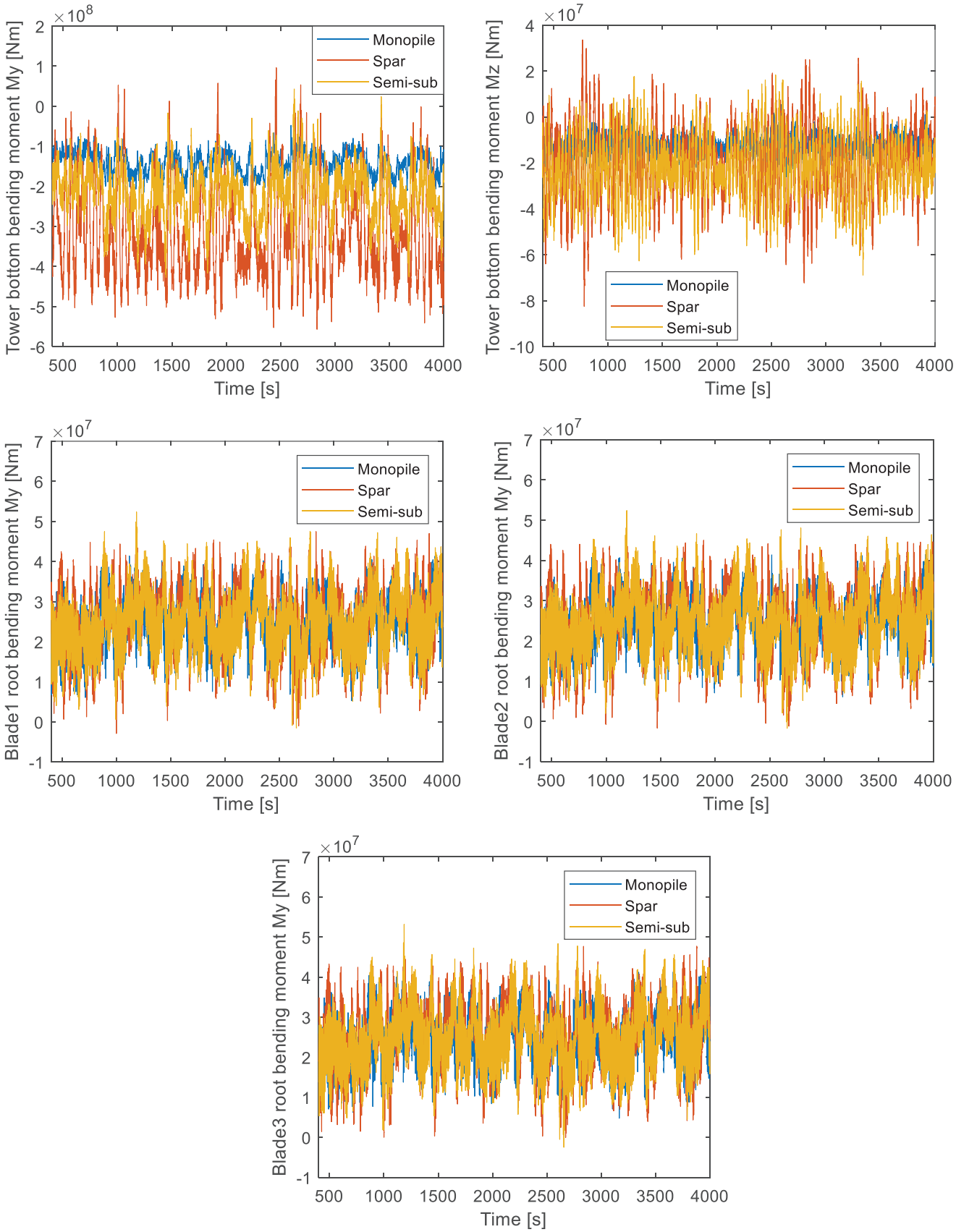

FIGURE 4 Example time-domain results. Top-left: Tower My bending moment. Top-right: Tower Mz bending moment. Centre-left: Blade 1 My bending moment. Centre-right: Blade 2 My bending moment; Bottom: Blade 3 My bending moment.

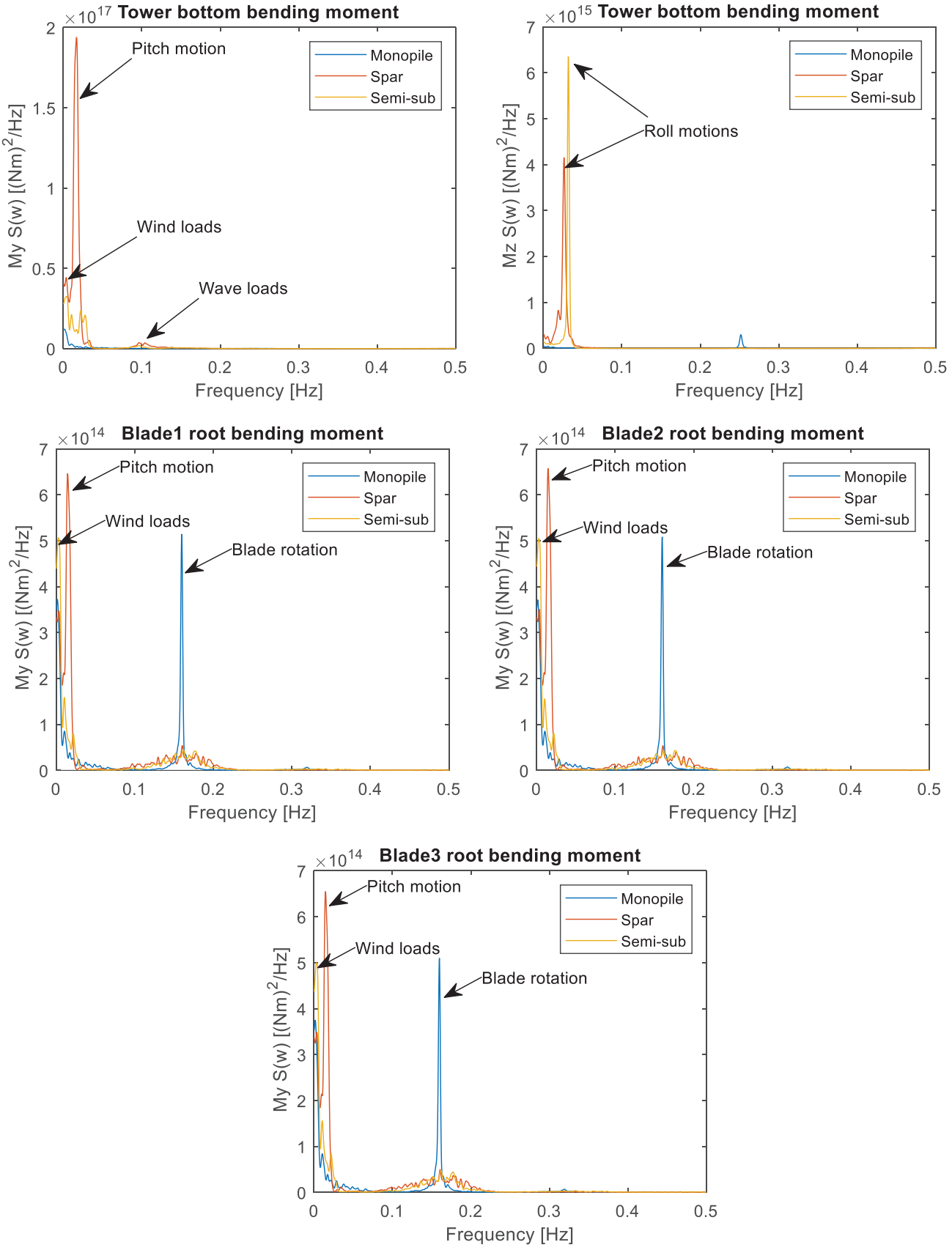

FIGURE 5 Power spectral distributions. Top-left: Tower My bending moment. Top-right: Tower Mz bending moment. Centre-left: Blade 1 My bending moment. Centre-right: Blade 2 My bending moment. Bottom: Blade 3 My bending moment.

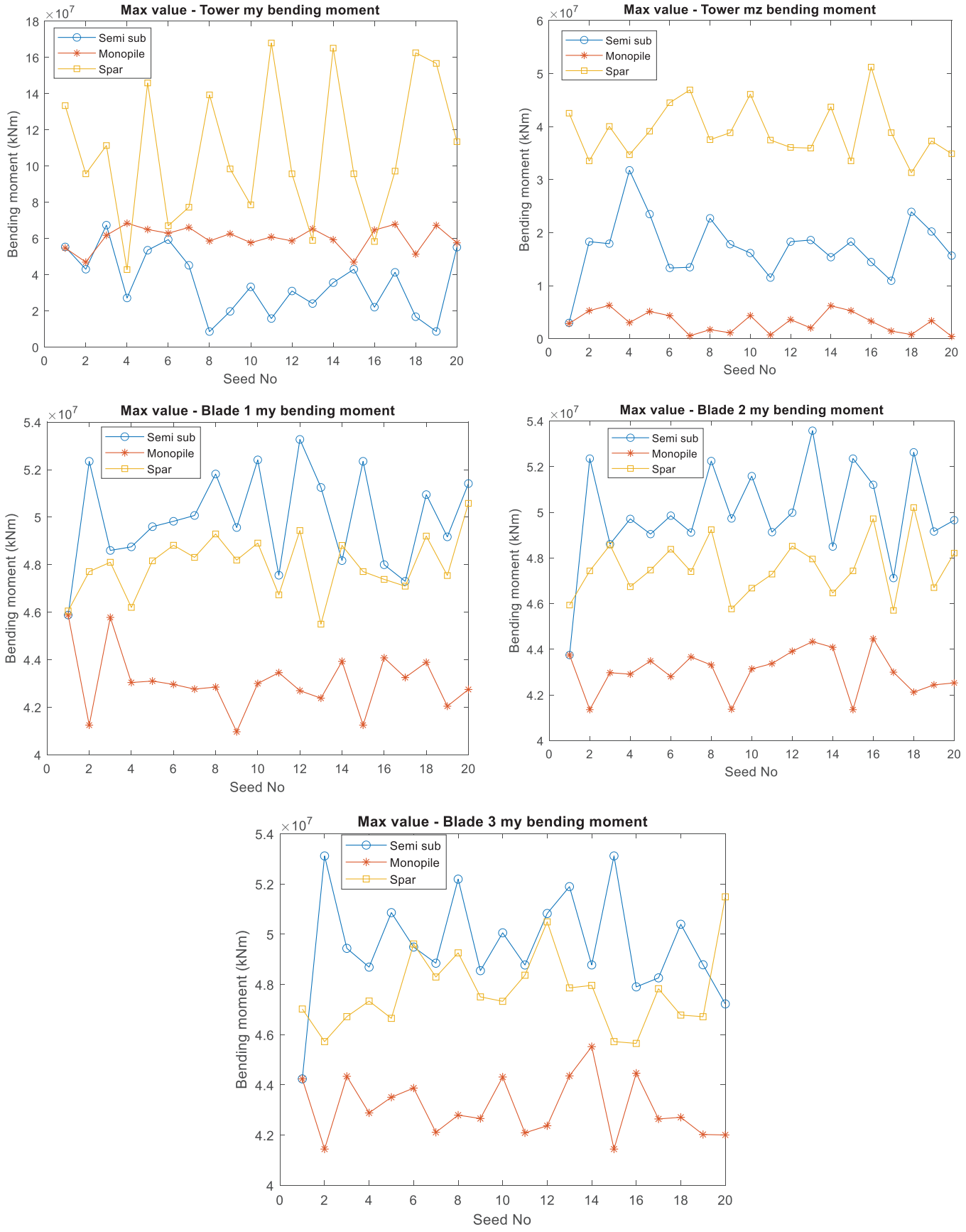

FIGURE 6 Maximum value in each realisation. Top-left: Tower My bending moment. Top-right: Tower Mz bending moment. Centre-left: Blade 1 My bending moment. Centre-right: Blade 2 My bending moment. Bottom: Blade 3 My bending moment.

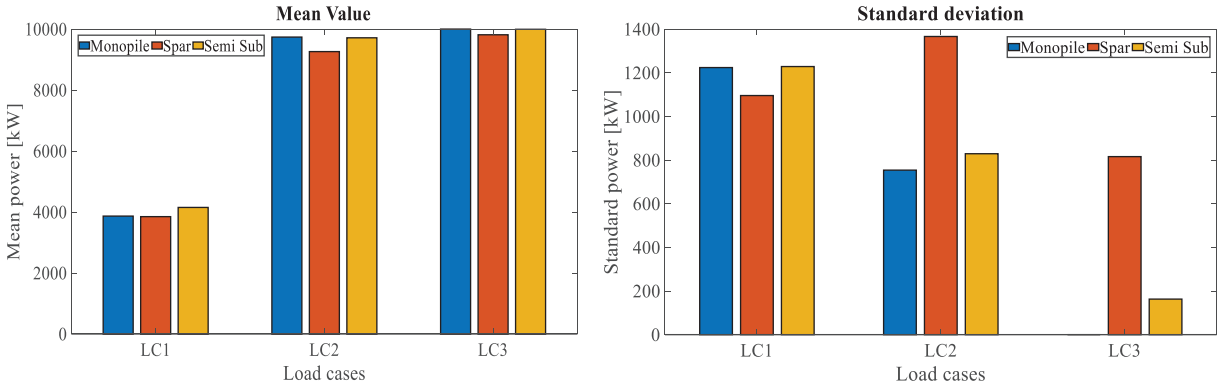

FIGURE 7 Power production of the monopole, spar and semisubmersible wind turbines. Left: Mean values. Right: Standard deviations.

It is observed that the standard deviations are generally large while the wind turbines are operating in the under-rated wind speed region. This is because the blade pitch controller is not active in this region, and the rotor will speed up or down accordingly to the incoming wind speed. This means the wind turbine has no control effort to limit the power fluctuations resulting from natural wind speed fluctuations. The standard deviations in the above-rated region are significantly smaller as the blade pitch controller is active and the wind turbines are limited at rated power. This means that the rotor speeds are constant in this region. For the fixed wind turbine, the rotor speed will be constant at the rated speed, and the wind turbine will produce at rated power without any noticeable power fluctuations. This explains the nearly zero standard deviation for the fixed wind turbine in LC3. The standard deviations in LC2 (rated wind speed) are larger than LC3 except for the spar wind turbine. This is because, in this region, the wind turbine is operating half the time in the under-rated wind speed region and the other half in the above-rated wind speed region. Therefore, the blade pitch controller is active half the time and helps to reduce the power fluctuations in the fixed and semisubmersible wind turbines. The spar wind turbine's smaller hydrostatic pitch restoring ability leads to significantly more significant standard deviations in the power production values. This is due to more significant platform pitch motions.

5.3 | Extreme load effects using ACER and Gumbel methods

5.3.1 | Example extrapolation plots

This section presents the extreme load responses using the ACER and Gumbel methods for the three operating conditions (LC1 – LC3) presented in Table 1. $K = 6$ is used. For illustration, the example plots of the ACER extrapolation and Gumbel fitting are presented in Figure 8.

As illustrated by the significantly smaller confidence intervals, the ACER method can lead to more accurate results as it does not assume a distribution. The ACER method does not assume any extreme value distribution. Instead, it follows the exact shape of the data points as presented in Figure 8. On the other hand, it is observed that the Gumbel distribution does fit the upper-end tail well. The data points tend to curve up towards the left for increasing response values and are above the Gumbel line. This means the Gumbel distribution will tend to overpredict the extreme value responses. This example shows the advantages of the ACER method.

TABLE 1 Load cases for numerical simulations [32].

Load cases	U_{hub} (m/s)	T_I	H_s (m)	T_p (s)	Samples	Simulation length (s)
LC1	8	0.1740	1.9	9.7	20	4000
LC2	12	0.1460	2.5	10.1	20	4000
LC3	16	0.1320	3.2	10.7	20	4000

The extreme load responses and the 95 % Cis from both ACER and Gumbel methods are also plotted in Figure 6 for the example presented. The numerical values of all results are presented in Tables 2 and 3 of the Appendix for extreme values calculated by the ACER and Gumbel methods, respectively.

6 | RESULTS AND DISCUSSIONS

The extreme values of the bending moments are presented in Figures 9–11 for the blade My bending moments and Figures 12 and 13 for the tower bending moments. In general, the loads at below-rated wind are the smallest, these increase to the maximum at the rated wind speed and taper off in the rated wind region. Like the power values presented in Section 5.2, the extreme values for the spar wind turbine are larger than the monopile and submersible wind turbines. Further, the extreme loads of all blades are similar.

6.1 | Below-rated wind

The blade extreme values for the monopile wind turbine are larger than the floating wind turbines. In this region, the pitch controller of the wind turbine is not active, and the rotor is allowed to adjust its speed freely to maintain an optimal tip

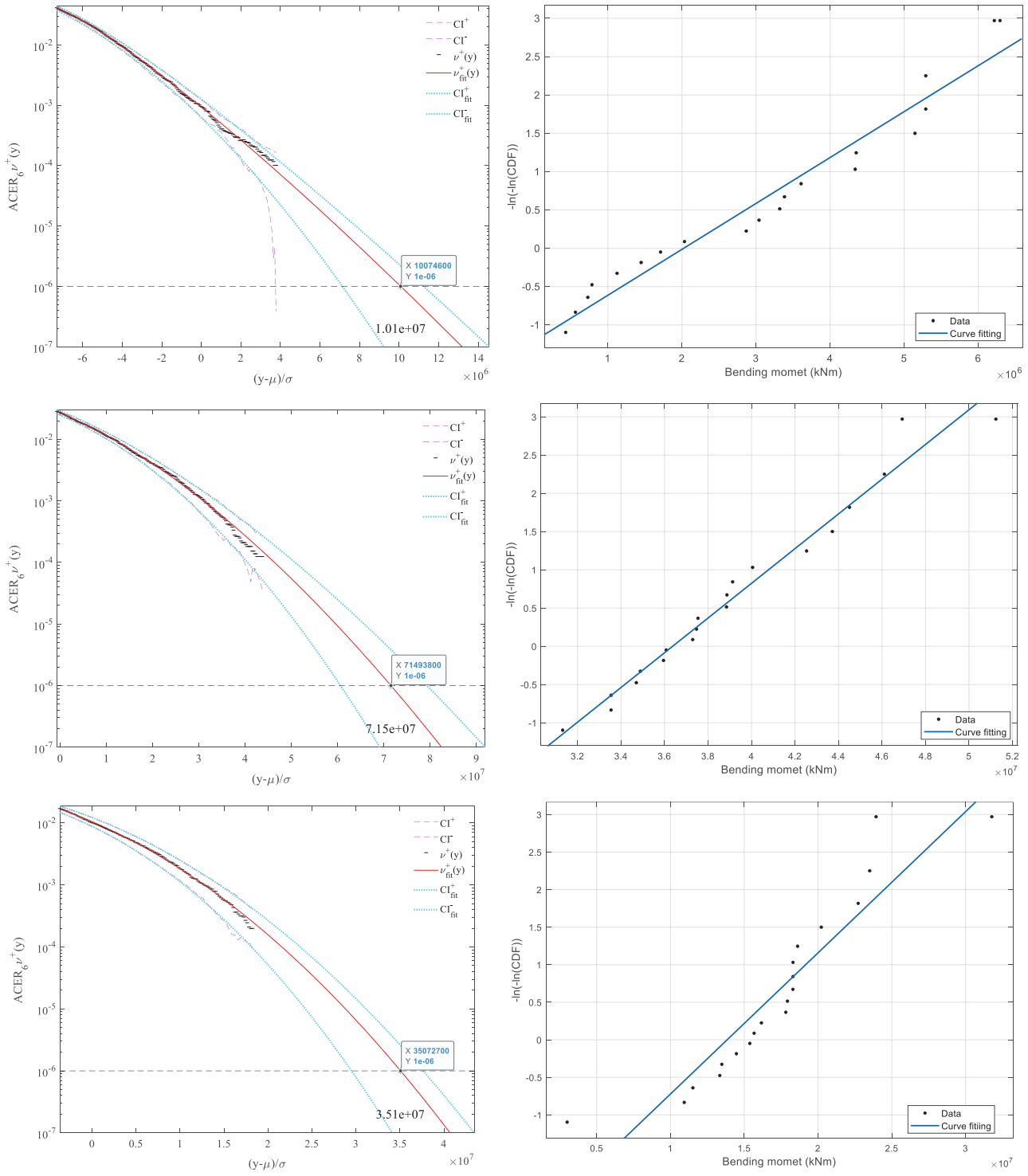

FIGURE 8 Example plot of ACER and Gumbel method LC 2: 12 m/s. Top-left: ACER Monopile Tower Mz bending moment. Top-right: Gumbel Monopile Tower Mz bending moment. Centre-left: ACER Spar tower Mz bending moment. Centre-right: Gumbel Spar tower Mz bending moment. Bottom left: ACER Semi-submersible tower Mz bending moment.; Bottom-right: Gumbel Semi-submersible tower Mz bending moment.

speed ratio. Since the monopile wind turbine is fixed to the ground, it will not experience any platform pitch motion, and therefore it will extract the full potential from the aerodynamic power exerted by the wind on it. On the other hand, platform pitch motions in the floating wind turbines lead to a slightly less optimal aerodynamic extraction power. Consequently, the aerodynamic loads will be larger for the monopile wind turbine, leading to larger blade extreme loads.

The tower bending moments My (fore-aft) are significantly higher in the floating wind turbines than the monopile wind turbine. This is due to platform pitch responses in the floating wind turbines. The larger platform pitch results

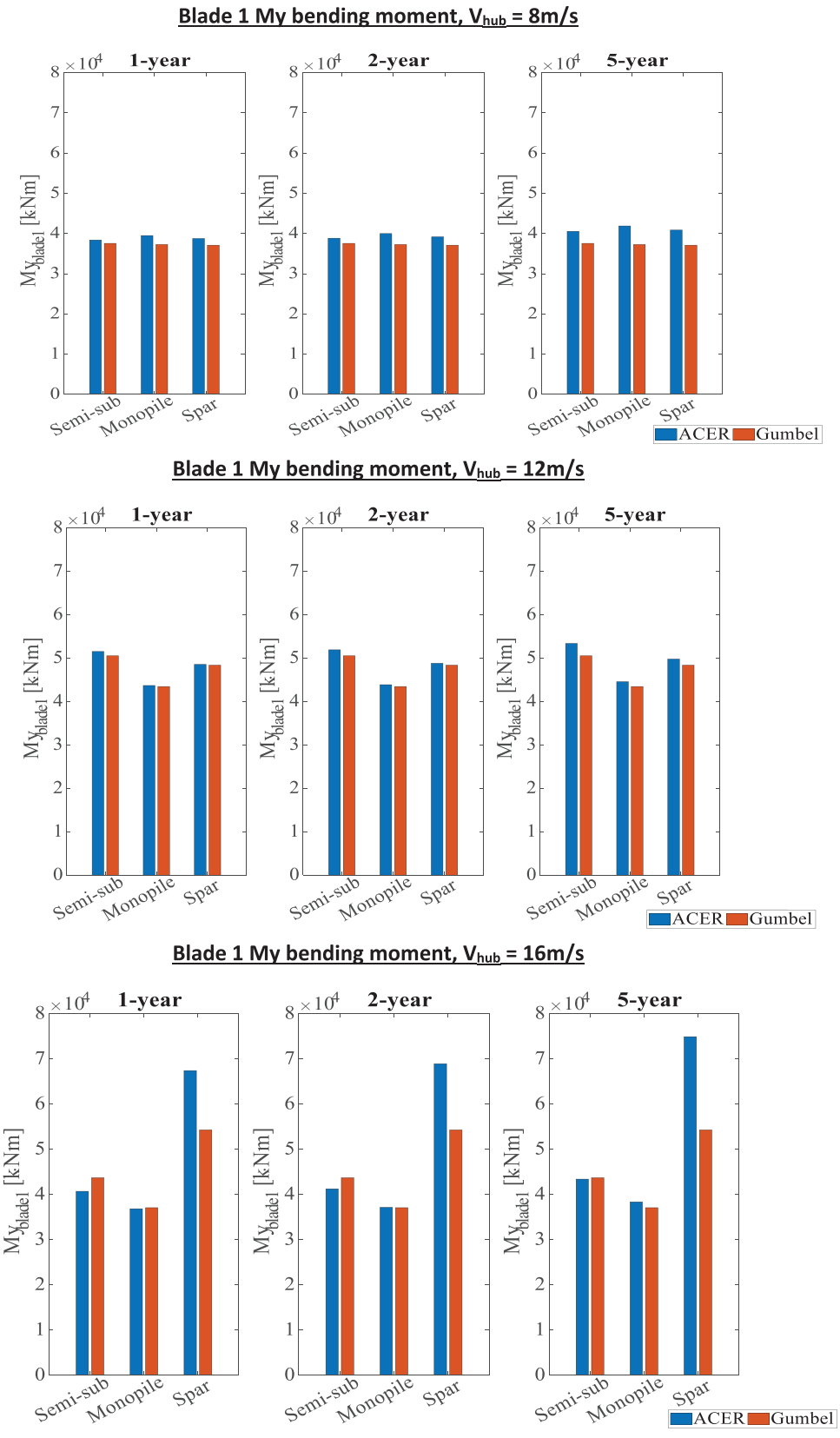

FIGURE 9 Extreme value responses of Blade 1 My bending moment.

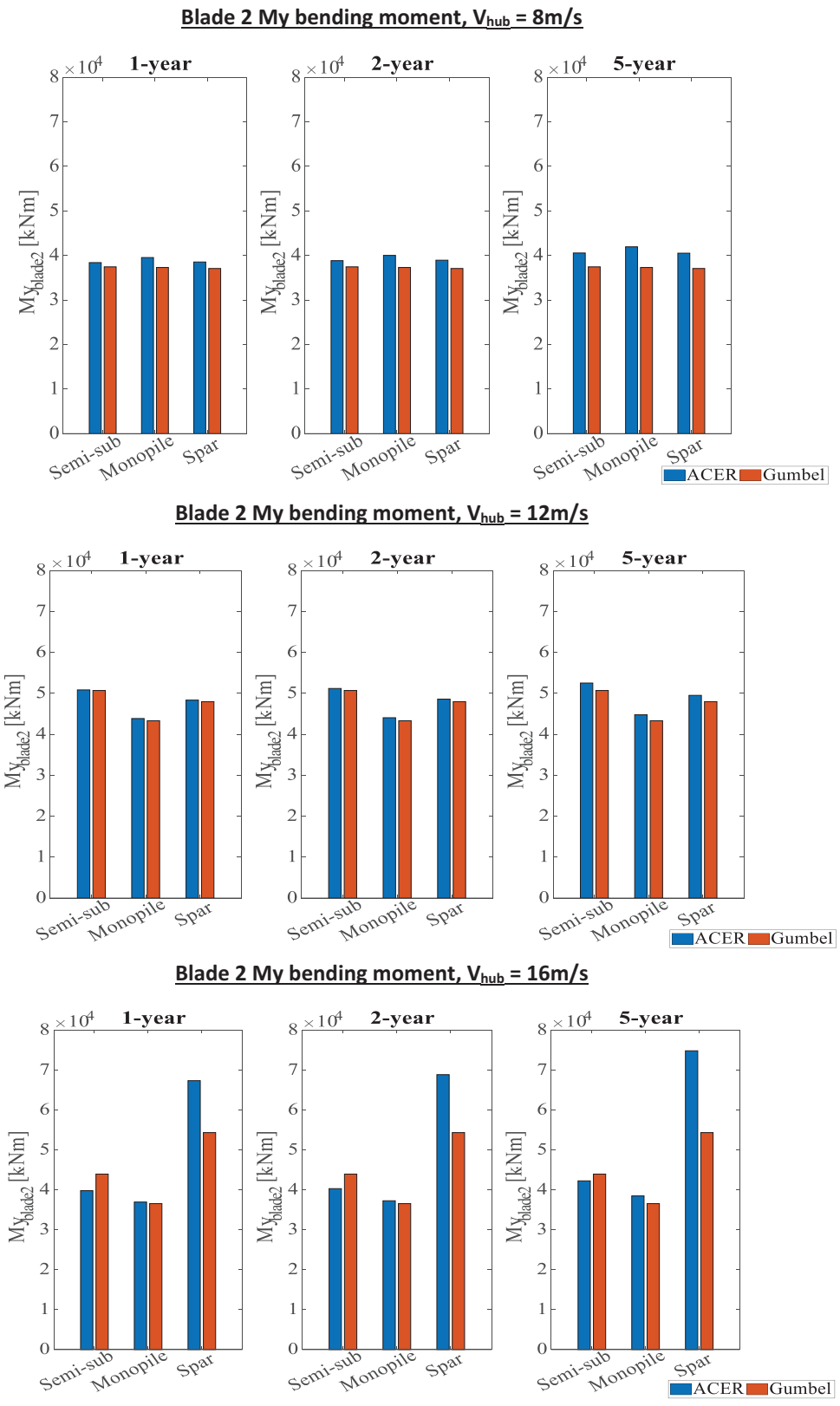

FIGURE 10 Extreme value responses of Blade 2 My bending moment.

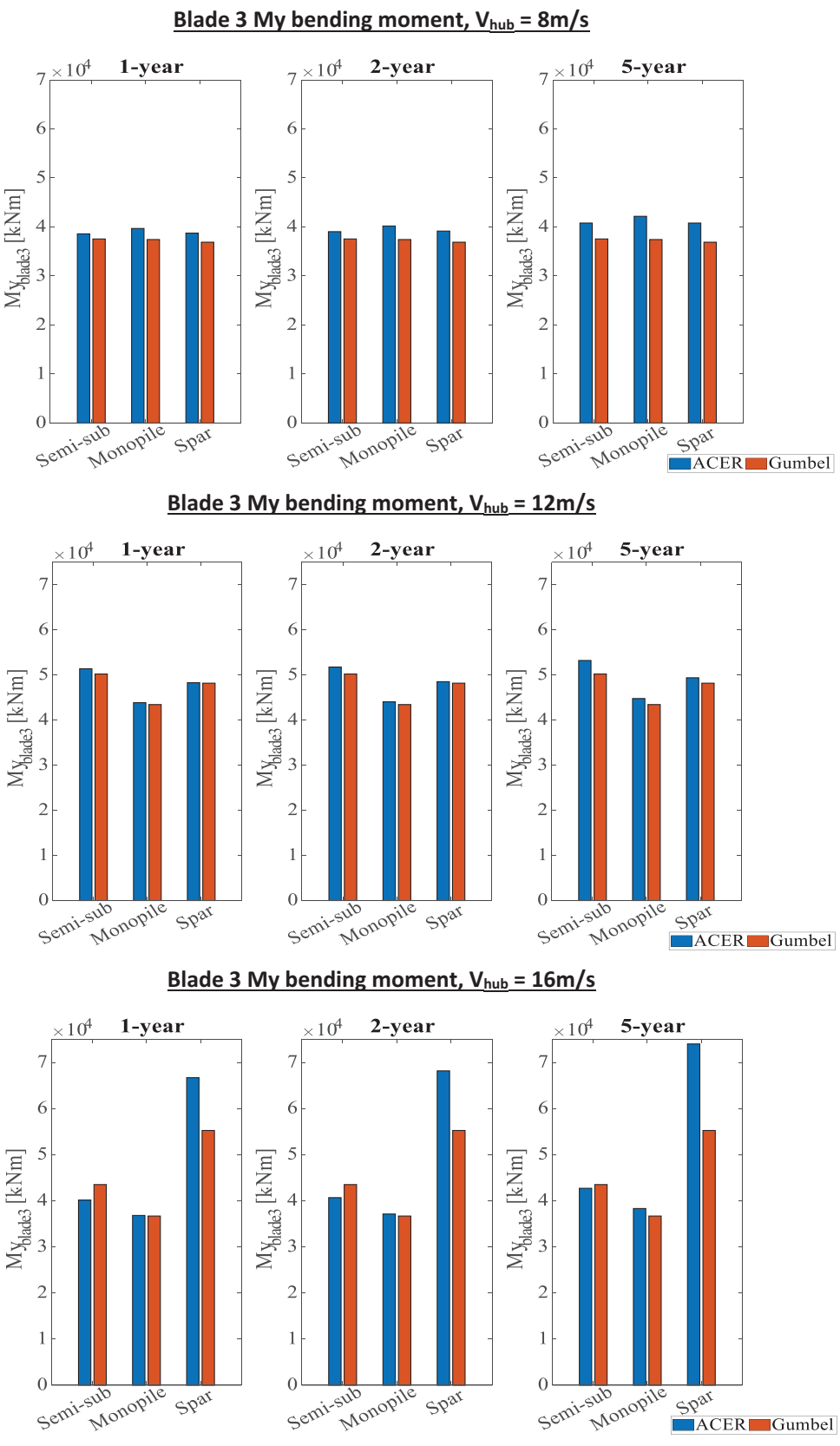

FIGURE 11 Extreme value responses of Blade 3 My bending moment.

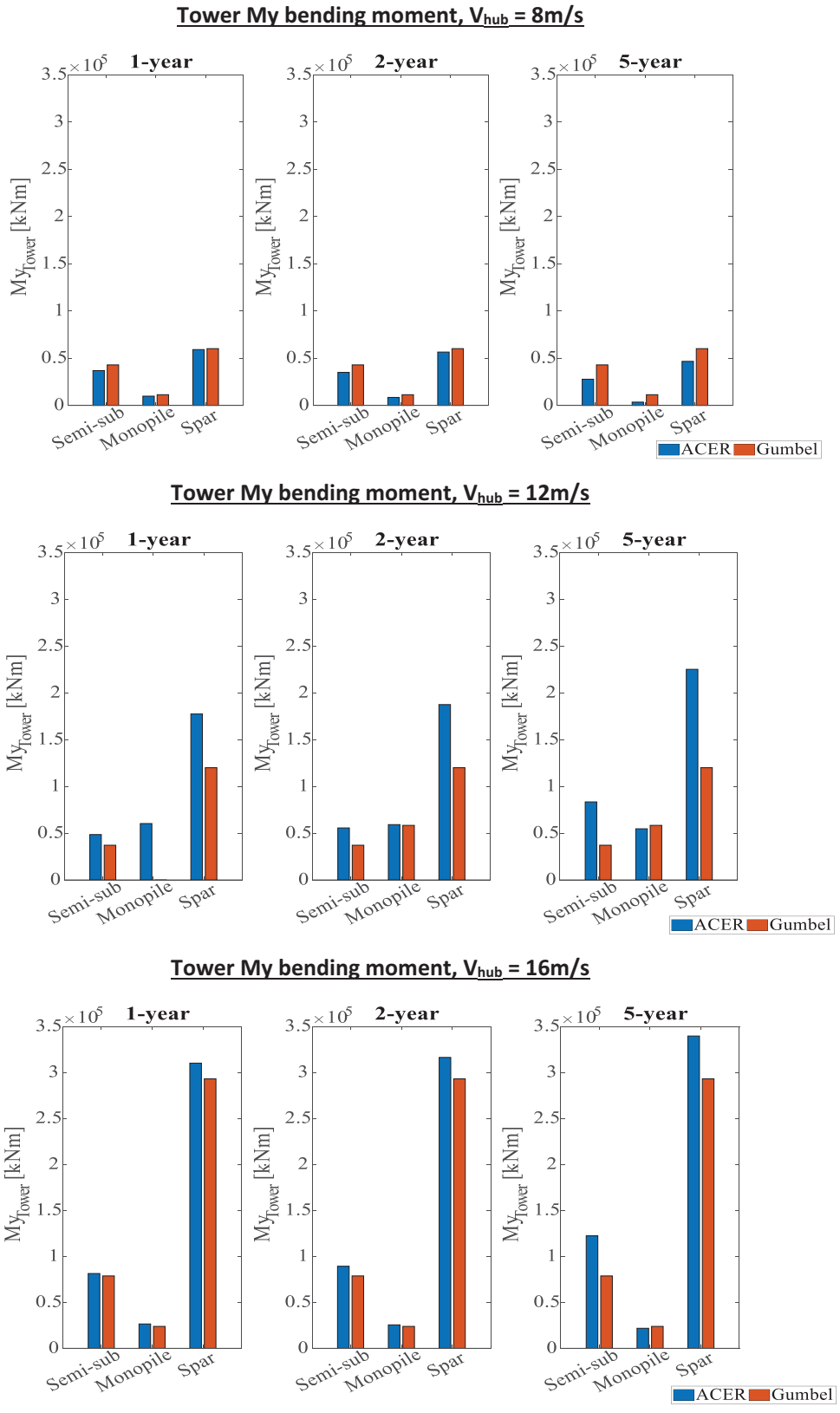

FIGURE 12 Extreme value responses of Tower My bending moment.

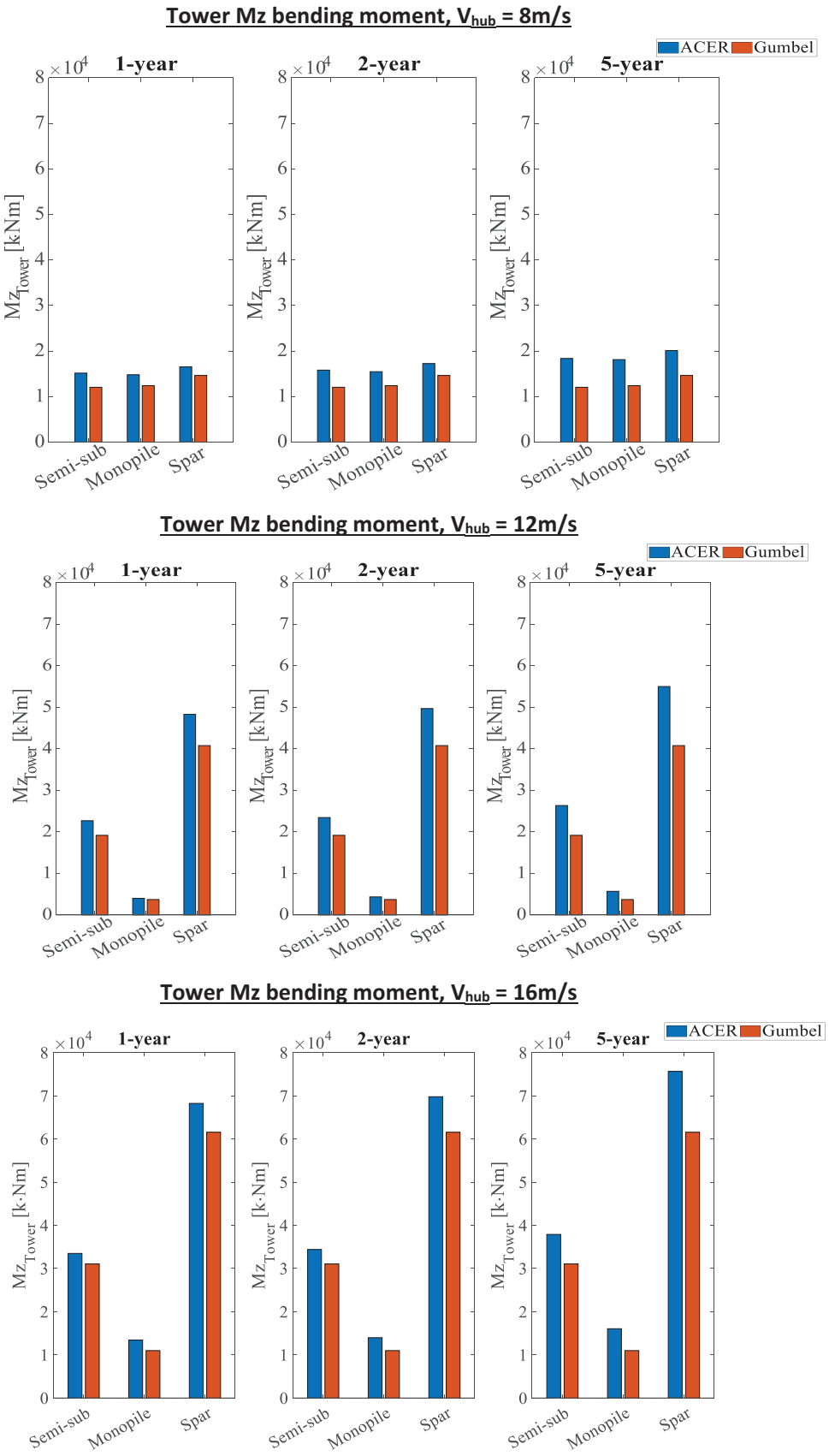

FIGURE 13 Extreme value responses of Tower Mz bending moment.

TABLE 2 Extreme value responses using ACER method for various return periods; 95 % confidence interval in paratheses.

Load case	Return period	1 year	2 years	5 years
	Exceedance probability, q	7.19×10^{-5}	5.71×10^{-5}	2.28×10^{-5}
LC1 V_{hub} = 8 m/s	RootMyb (kNm)	30726 (29149, 31682)	31084 (29393, 32082)	32479 (30315, 33645)
	LSSTipMys (kNm)	9245 (8673, 9616)	9390 (8792, 9768)	9937 (9241, 10351)
	TwrBsMyt (kNm)	328555 (318797, 336312)	332314 (322130, 340328)	346662 (334792, 355663)
LC2 V_{hub} = 12 m/s	RootMyb (kNm)	41445 (40752, 42073)	41662 (40934, 42338)	42485 (41615, 43372)
	LSSTipMys (kNm)	15061 (14140, 15677)	15327 (14349, 15973)	16357 (15136, 17122)
	TwrBsMyt (kNm)	437049 (428032, 444853)	439643 (429627, 446865)	449561 (436751, 457982)
LC3 V_{hub} = 16 m/s	RootMyb (kNm)	33406 (32141, 34231)	33790 (32440, 34657)	35293 (33587, 36335)
	LSSTipMys (kNm)	17054 (16567, 17449)	17282 (16780, 17688)	18144 (17584, 18591)
	TwrBsMyt (kNm)	359140 (343069, 367411)	364244 (347041, 372826)	384245 (362296, 394070)

TABLE 3 Extreme value responses using Gumbel method for various return periods; 95 % confidence interval in parentheses.

Load case	Return period	1 year	2 years	5 years
	Exceedance probablity, q	7.19×10^{-5}	5.71×10^{-5}	2.28×10^{-5}
LC1, V_{hub} = 8 m/s	RootMyb (kNm)	29772 (23844, 37194)	29772 (22344, 37194)	29772 (23844, 37195)
	LSSTipMys (kNm)	9061 (6870, 11953)	9061 (6870, 11953)	9061 (6870, 11953)
	TwrBsMyt (kNm)	314083 (229636, 429680)	314083 (229636, 429680)	314084 (229636, 429681)
LC2, V_{hub} = 12 m/s	RootMyb (kNm)	41593 (28380, 61026)	41593 (28380, 61026)	41593 (28380, 61026)
	LSSTipMys (kNm)	15321 (11801, 19903)	15321 (11801, 19904)	15321 (11801, 19904)
	TwrBsMyt (kNm)	491364 (368347, 655777)	491364 (368347, 655778)	491365 (368348, 655779)
LC3, V_{hub} = 16 m/s	RootMyb (kNm)	46542 (36896, 58215)	46542 (37218, 58215)	46542 (37218, 58215)
	LSSTipMys (kNm)	17168 (13676, 21530)	17168 (13676, 21530)	17168 (13676, 21530)
	TwrBsMyt (kNm)	466508 (384880, 566002)	466510 (384880, 566003)	466510 (384882, 566004)

in increased bending moment acting on the tower bottom due to nacelle tilt. The tower bending moment Mz (side-side) for all three platforms are similar. This is because all three wind turbines experience similar aerodynamic shear forces.

6.2 | Rated wind

In this region, the wind turbine is operating half the time in the below-rated (blade pitch controller not active) and the other half in the rated wind region (blade pitch controller active).

The blade pitch controller regulates the rotor speed when the above-rated wind speed. This reduces the wind turbine aerodynamic loads and, in general, will also reduce loads at other parts of the wind turbine. In the case of the monopile wind turbine, the effectiveness of the blade pitch controller is not affected by any platform pitch motion (since the turbine is fixed to the ground), and therefore, almost all of the controller effort is used in power regulation. This leads to lower blades and tower loads in the monopile wind turbine.

For the floating wind turbines, namely the spar and semisubmersible wind turbines, the effectiveness of the blade pitch controller is hampered by the platform pitch motion. The spar wind turbine has more significant platform pitch motions and is more affected. This leads to larger extreme loads for the spar wind turbine than the semisubmersible wind turbine for both blades and tower loads.

6.3 | Above-rated wind

In this region, the blade pitch controller is constantly active. Therefore, the combined effect of the blade pitch controller and the platform pitch motions on wind turbine loads will be even more prominent compared to in the rated-wind region.

The extreme loads on the monopile wind turbine are slightly lower than the loads in the rated-wind region. This is obvious as the blade pitch controller is acting to reduce aerodynamic loads all the time in this region. Note that even though there are larger waves (due to higher wind speeds) in this region, the wave loads on the monopile wind turbine are smaller than the wind loads.

The combined effect of the blade pitch controller and the platform pitch motions on the extreme loads is significant, particularly for the spar wind turbine. It is observed that the loads in the spar wind turbine are significantly larger for both the blade and tower.

6.4 | ACER vs Gumbel

The extreme values presented using the ACER method are higher than the Gumbel method. However, 95% Cis of the values predicted from the ACER method are significantly narrower than the 95% Cis of the values predicted from the Gumbel method. This means that the ACER method is more accurate and highlights the benefits of the ACER in not assuming a distribution in the extrapolation of extreme values. Further, this indicates that the Gumbel distribution does not fit the extreme value responses very well. In addition, the 1, 2, and 5-year extreme values calculated using the Gumbel method are similar. This is due to the inaccurate fit of the probability distribution at the upper tail end. The fitted Gumbel probability density distribution slope is too steep at the upper tail end. This leads to minimal changes in the response values for a unit change in probability. The 1, 2 and 5-year extreme values are generally 1.1-1.3 times larger than the maximums of single 1-h realisations. The relatively large range of values (about 20%) indicates the importance of using accurate extrapolation methods to predict extreme values that can be used to define appropriate design values utilised in deterministic engineering design.

7 | CONCLUSIONS

This paper investigated the power performance and extreme responses for three 10-MW offshore wind turbines, that is, a bottom-fixed monopile turbine, a spar-type and a semisubmersible floating wind turbines. The ACER and Gumbel methods are used to predict the extreme responses. The responses are based on fully coupled nonlinear numerical analysis, including structural flexibility, aero, hydrodynamics, control dynamics, interaction with combined turbulent wind and stochastic waves.

The mean power performance of the three OWTs are close under the below-rated, rated, and above-rated operating conditions, while the standard deviations of the spar turbine are obviously larger than those of the monopile and semisubmersible turbines, which is due to the large pitch motion of the spar-type floating wind turbine. The standard deviations of power performance are generally smallest in the above-rated condition in the three representative operating range, which is because of the pitch controller effect to limit the power fluctuations.

In general, the extreme loads of the spar wind turbine are larger than the monopile and submersible wind turbine, particularly for the rated and above-rated wind conditions. The extreme blade loads are similar in the below-rated and rated wind regions. In the above-rated region, the extreme blade loads for the spar wind turbine are significantly larger than the monopile and semisubmersible. The extreme blade loads of the submersible wind turbine are slightly larger than the monopile wind turbine. The extreme tower bending loads of the spar is the largest in all operating regions, followed by the semisubmersible wind turbine and the monopile wind turbine.

The 1, 2 and 5-year responses of the FOWT were, in general, 1.1–1.3 times larger than the maximums of single 1-h realisations. This reinforces the importance of using extrapolation methods to determine extreme loads to be used as ULS loads. The ACER results have a smaller 95% CI than the Gumbel results. This means the ACER method is more accurate than the Gumbel method. The Gumbel method's 1, 2 and 5-year responses are quite similar. This is due to poor Gumbel fitting of the data at the upper tail. On the other hand, the ACER does not assume any distributions and therefore does not have the same poor fit issue at the tail end. The better performance of the ACER method is because, in contrast to Gumbel, it does not assume that the extreme responses follow a designated probability distribution.

The present work mainly focuses on the power performance and dynamic characteristics in term as extreme responses of the three representative OWTs, it is of great interest to conduct the economic analysis of the various types of OWTs considering the design, construction, installation, transportation, installation, inspection and maintenance etc., throughout the entire lifetime.

AUTHOR CONTRIBUTIONS

Shuaishuai Wang: Conceptualization, Methodology, Software, Formal analysis, Investigation, Writing-original draft, Writing-review & editing, Visualization; **Yihan Xing**:Conceptualization, Methodology, Formal analysis, Investigation, Writing-original draft, Visualization, project administration; **Anuraj Karuvathil**: Software, Formal analysis, Writing-original draft. **Oleg Gaidai**: Methodology, Formal analysis, Resources.

CONFLICT OF INTEREST STATEMENT

The authors declare no conflict of interest.

DATA AVAILABILITY STATEMENT

The data that support the findings of this study are available from the corresponding author upon reasonable request.

ORCID

Yihan Xing https://orcid.org/0000-0003-0883-4854

REFERENCES

1. Wind Europe: Offshore Wind in Europe: Key Trends and Statistics 2020
2. International Electrotechnical Commission: Offshore Wind Outlook (2019) https://www.iea.org/reports/offshore-wind-outlook-2019
3. Musial, W., Beiter, P., Tegen, S., Smith, A.: Potential Offshore Wind Energy Areas in California: An Assessment of Locations, Technology, and Costs (No. NREL/TP-5000-67414). National Renewable Energy Lab. (NREL), Golden, CO (2016)
4. International Electrotechnical Commission: Wind Turbines-Part 3: Design Requirements for Offshore Wind Turbines, 61400–3 (2009)

5. Zhang, L., Shi, W., Zeng, Y., Michailides, C., Zheng, S., Li, Y.: Experimental investigation on the hydrodynamic effects of heave plates used in floating offshore wind turbines. Ocean Eng. 267, 113103 (2023)
6. Souza, C.E.S., Bachynski, E.E.: Changes in surge and pitch decay periods of floating wind turbines for varying wind speed. Ocean Eng. 180, 223–237 (2019)
7. Wise, A.S., Bachynski, E.E.: Wake meandering effects on floating wind turbines. Wind Energy. 23(5), 1266–1285 (2020)
8. Shi, W., Zhang, L., Karimirad, M., Michailides, C., Jiang, Z., Li, X.: Combined effects of aerodynamic and second-order hydrodynamic loads for floating wind turbines at different water depths. Appl. Ocean Res. 130, 103416 (2023)
9. Johlas, H.M., Martínez-Tossas, L.A., Churchfield, M.J., Lackner, M.A., Schmidt, D.P.: Floating platform effects on power generation in spar and semisubmersible wind turbines. Wind Energy 24(8), 901–916 (2021)
10. Aggarwal, N., Manikandan, R., Saha, N.: Nonlinear short term extreme response of spar type floating offshore wind turbines. Ocean Eng. 130, 199–209 (2017)
11. Chen, X., Jiang, Z., Li, Q., Li, Y., Ren, N.: Extended environmental contour methods for long-term extreme response analysis of offshore wind turbines. J. Offshore Mech. Arct. Eng. 142(5), 052003 (2020)
12. Naess, A., Moan, T.: Stochastic Dynamics of Marine Structures. Cambridge University Press, New York (2013)
13. Næss, A., Gaidai, O.: Estimation of extreme values from sampled time series. Struct. Saf. 31(4), 325–334 (2009)
14. Ahmad, U.N., Xing, Y., Wang, S.: Determination of extreme responses of USFG's equilibrium glide path hovering in ocean current. Ocean Eng. 263, 112343 (2022)
15. Balakrishna, R., Gaidai, O., Wang, F., Xing, Y., Wang, S.: A novel design approach for estimation of extreme load responses of a 10-MW floating semi-submersible type wind turbine. Ocean Eng. 261, 112007 (2022)
16. Gaidai, O., Xing, Y., Wang, F., Wang, S., Yan, P., Næss, A., Improving extreme anchor tension prediction of a 10-MW floating semi-submersible type wind turbine, using highly correlated surge motion record (2022)
17. Xu, X., Gaidai, O., Naess, A., Sahoo, P.: Extreme loads analysis of a site-specific semisubmersible type wind turbine. Ships Offshore Struct. 15(sup1), S46–S54 (2020)
18. Bak, C., Zahle, F., Bitsche, R., Kim, T., Yde, A., Henriksen, L.C., …, Natarajan, A.: The DTU 10-MW reference wind turbine. Paper presented at Danish wind power research, TrinityGl, Fredericia, 27–28 May 2013
19. Velarde, J., Bachynski, E.E.: Design and fatigue analysis of monopile foundations to support the DTU 10 MW offshore wind turbine. Energy Procedia 137, 3–13 (2017)
20. Hegseth, J.M., Bachynski, E.E.: A semi-analytical frequency domain model for efficient design evaluation of spar floating wind turbines. Mar. Struct. 64, 186–210 (2019)
21. Jonkman, J., Definition of the Floating System for Phase IV of OC3 (No. NREL/TP-500-47535). National Renewable Energy Lab. (NREL), Golden, CO (2010)
22. Yu, W., Müller, K., Lemmer, F., Bredmose, H., Borg, M., Sanchez, G., Landbo, T., Public definition of the two LIFES50+ 10MW floater concepts. LIFES50+ Deliverable, 4 (2017)
23. Pegalajar-Jurado, A., Madsen, F.J., Borg, M., Bredmose, H.: State-of-the-art models for the two LIFES50+ 10 MW floater concepts. Tech. Rep. 4 (2018)
24. Wang, S.: Design and Dynamic Analysis of a 10-MV Medium-Speed Drivetrain in Offshore Wind Turbines (2021)
25. SIMA: Marine operations and mooring analysis software. https://www.dnv.com/services/marine-operations-and-mooring-analysis-software-sima-2324. Accessed 7 March 2022
26. Cheng, Z., Madsen, H.A., Chai, W., Gao, Z., Moan, T.: A comparison of extreme structural responses and fatigue damage of semisubmersible type floating horizontal and vertical axis wind turbines. Renew. Energy 108, 207–219 (2017)
27. Xu, K., Zhang, M., Shao, Y., Gao, Z., Moan, T.: Effect of wave nonlinearity on fatigue damage and extreme responses of a semisubmersible floating wind turbine. Appl. Ocean Res. 91, 101879 (2019)
28. Naess, A., Gaidai, O., Teigen, P.S.: Extreme response prediction for nonlinear floating offshore structures by Monte Carlo simulation. Appl. Ocean Res. 29(4), 221–230 (2007)
29. Chai, W., Naess, A., Leira, B.J., Bulian, G.: Efficient Monte Carlo simulation and Grim effective wave model for predicting the extreme response of a vessel rolling in random head seas. Ocean Eng. 123, 191–203 (2016)
30. Peeringa, J.M.: Comparison of Extreme Load Extrapolations Using Measured and Calculated Loads of a MW Wind Turbine. Energy Research Centre of the Netherlands (ECN), Petten (2009)
31. Lott, S., Cheng, P.W.: Load extrapolations based on measurements from an offshore wind turbine at alpha ventus. J. Phys.: Conf. Series 753(7), 072004 (2016)
32. Li, L., Gao, Z., Moan, T.: Joint environmental data at five european offshore sites for design of combined wind and wave energy devices. In: International Conference on Offshore Mechanics and Arctic Engineering, vol. 55423, p. V008T09A006. American Society of Mechanical Engineers, New York (2013)

How to cite this article: Wang, S., Xing, Y., Karuvathil, A., Gaidai, O.: A comparison study of power performance and extreme load effects of large 10-MW offshore wind turbines. IET Renew. Power Gener. 1–20 (2023). https://doi.org/10.1049/rpg2.12721